P. A. Bhounsule, Control based on passive dynamic walking, Bioinspired Legged Locomotion: Models, Concepts, Control and Applications, 1st edition, Editors: Maziar Sharbafi and Andre Seyfarth. Publisher: Elsevier, Butterworth-Heinemann, 2017, ISBN. 9780128037744 (Book chapter)

Control based on passive dynamic walking

Author: Pranav A. Bhounsule
Email: pranav.bhounsule@utsa.edu
Affiliation: Dept. of Mechanical Engineering, University of Texas San Antonio,
Address: 1 UTSA Circle, San Antonio, TX 78249, USA.

1.1 Abstract

Passive dynamic walking robots are machines that use only their natural dynamics – mass distribution and geometry – to move downhill. Since these robots use no external actuators, they are highly energy-efficient. But the most striking aspect is that their motion looks natural and graceful resembling that of a human. These passive dynamic slope walkers have provided inspiration for minimally powered dynamic walkers. The minimally powered walkers use their actuators to guide and shape the natural dynamics thereby retaining the energy efficiency and fluidity of the fully passive walkers.

We first introduce concepts such as Poincare map, Limit cycle, Eigenvalue-based stability which are key in analyzing passive dynamic walking-based robots. We illustrate these concepts by analyzing the simplest 2D dynamic walking model going downhill without any control. The results indicate that there are stable motions of the simplest 2D walker. Next, we present how minimal control can be used to create almost passive walking robots on level ground. Some of the control methods discussed are: virtual gravity control that mimics gravity encountered on a downhill ramp, tracking the mechanical energy of passive dynamic walkers, on-off or bang-bang control to supply energy lost during foot-strike, low-gain position control using set points to guide the swing leg, and a discrete, event-based, intermittent controller to modulate desired outputs over one or multiple steps. We give a commentary on current state-of-art of powered passive dynamic robots with respect to energy-efficiency, stability, robustness, versatility, mechanical design, estimation, and robot complexity. We conclude that although passive dynamic robots are energy efficient, they have shown limited proficiency on metrics of stability, robustness, and versatility. Thus, the grand challenge in this area is to create machines that are adept at the afore-mentioned metrics without compromising on the energy-efficiency.
Keywords: Passive Dynamic Walking, Compass gait, Poincaré maps, Limit cycle, Natural Dynamics, Cost of Transport.

1.2 Introduction

How much control is needed to create walking gaits for legged robots? The passive dynamic walking paradigm suggests that movement in a legged robot requires no control because walking can emerge purely from the mechanics of the legs. Passive dynamic walking robots are machines that use their natural dynamics, i.e., their mass distribution and geometry, to move downhill with no actuation or control.

The concept of passive dynamic walking is about a century old as evidenced by a number of patents on downhill walking toys (Fallis 1888 [19], Bechstein 1912 [3], Mahan 1909 [36], and Wilson 1938 [49]). The Wilson Walker is shown in Fig. 1.1 (a). It has two legs, each of which connects to a body by a hinge joint. When launched correctly, the toy is able to walk stably down a slight incline. Specifically, the side-ways rocking of the body lifts a foot off the ground. The off-ground foot then swings forward to complete a step. The same sequence is repeated with the other foot, thus enabling steady downhill locomotion.

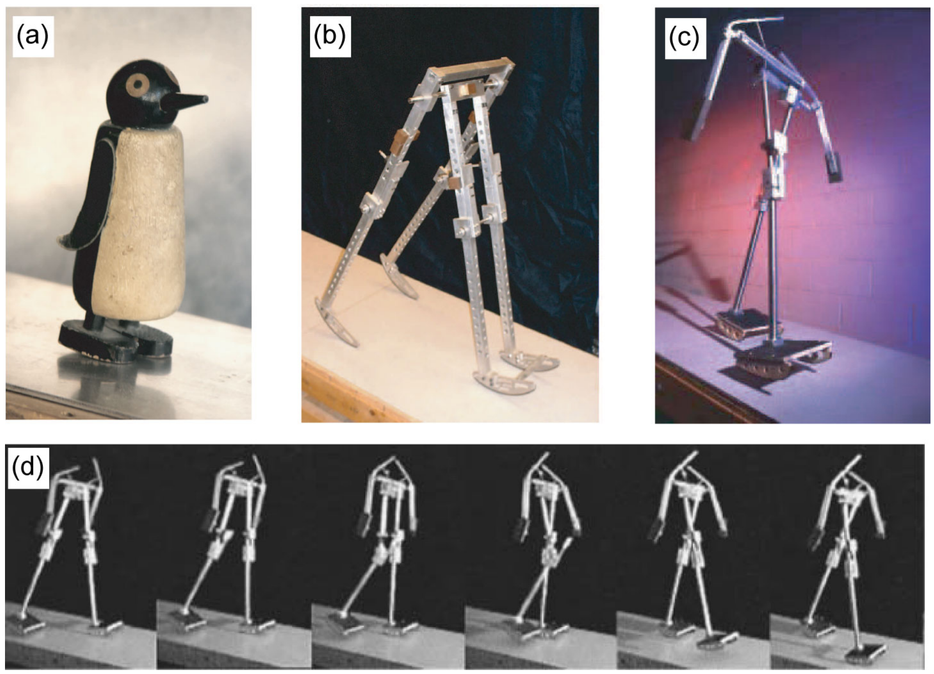

Figure 1.1: (a) The Wilson walker, (b) A copy of McGeer's passive dynamic walker built at Cornell University, (c) A 3D passive dynamic walker with arms from Cornell University. These figures are from [15]. (d) A sequence of snapshots during walking of the 3D passive dynamic walker shown in c. The figure is from [17].

The Wilson walker inspired McGeer [38] to create the first passive dynamic walking machine. His robot, called the Dynamite, had four legs with knees but arranged in pairs so that the inner two and outer two legs alternate during walking (see Fig. 1.1 (b) for a replica made at Cornell University). Like the Wilson walker, Dynamite was able to walk stably downhill when launched with the right set of initial conditions. But the configuration of the legs limits the walking only to the sagittal or the front-back plane. Collins et al. [17] created a 3D passive dynamic robot with two kneed legs and two swinging arms (see Fig. 1.1 (c) and (d)).

Their design had swinging arms coupled to the legs and feet with guide rails to stabilize side-to-side (roll motion) and turning (yaw motion). Owaki et al. [44] built the first successful passive dynamic running robot. Their design had four legs with knees arranged in pairs (two inner- and outer- legs coupled to each other), an axial spring in each of the legs to cushion collisions, a spring between the legs to aid hip swing, and arc shaped feet. The robot was able to successfully run 36 steps on downhill ramp with slope of 0.22 rad. All these robots have the common feature that they use their natural dynamics and gravity to descend downhill. Since these robots use no motors, they are very energy-efficient. However, the most striking aspect is that their motion looks natural and graceful like that of human. Indeed, Mochon and McMahon [41] have shown that the leg swing in human walking is dictated greatly by the natural dynamics with very little control. This suggests that perhaps humans exploit their natural dynamics to walk while expending negligible amounts of energy. We think that these two aspects, the energy-efficiency and the biological relevance, makes it appealing and interesting to study the role of passive dynamics in creating functional legged robots.

The rest of the chapter is written as follows. We describe the simplest passive dynamic walker in Sec. 1.3 and provide necessary details for analyzing its motion. This model is a nice starting point for beginners in the field. Next in Sec. 1.4, we describe techniques to enable passive-dynamic walking on level ground with or without control. The discussion and challenges in creating passive-dynamics based robots are in Sec. 1.5. Finally, the conclusions follow in Sec. 1.6.

1.3 Passive dynamic walking on a slope

The first known simulation of a passive dynamic walking model was done by McGeer [38]. Two other well-known papers are those by Goswami et al. [27], who called it the compass-gait walker (reminiscent of the compass tool used in drawing), and by Garcia et al. [22], who created an extremely simplified model and called it the simplest walker. Garcia's model had a point mass at the hip and massless legs. After non-dimensionalizing velocity, the model has a single parameter, the ramp slope. The simplicity of this model makes it very attractive for learning about passive dynamic models. We present the analysis used in Garcia et al. [22] in the next section. The MATLAB code for simulating the simplest walker and for general mass distribution round feet walker is available in the paper by Bhounsule [6]. Another tutorial paper on passive dynamics is by Wisse and Schwab [51].

1.3.1 Model description and equations of motion

Figure 1.2 (ii) shows a model of the simplest walker. The model consists of a mass M at the hip and a point mass m at each of the two feet. Each leg has length ℓ, gravity g points downwards, and the ramp slope is γ. The leg in contact with the ramp is called the stance leg (thin red line) while the other leg is called the swing leg (thick blue line). The angle made by the stance leg with the normal to the ramp is θ (counter-clockwise is positive) and the angle made by the swing leg with the stance leg is ϕ (clockwise is positive). Figure 1.2 a single walking step for the walker. The walker starts in (i), the state in which the front leg is the stance leg and the trailing leg is the swing leg. A sequence of snapshots that make up a single step are shown from (ii) to (v). Finally in (vi), the swing leg collides with the ground and becomes the new stance leg. At this point, we have a complete gait cycle, i.e., the walker configuration in (vi) is the same as (i). Note that between (iii) and (iv), there is foot scuffing because the swing leg passes through the ground. We ignore foot scuffing in the model but an experimental prototype needs to have a mechanism to create foot clearance during swing. Foot clearance can be created by having actuated ankles [7] or by adding knees to the walker [39].

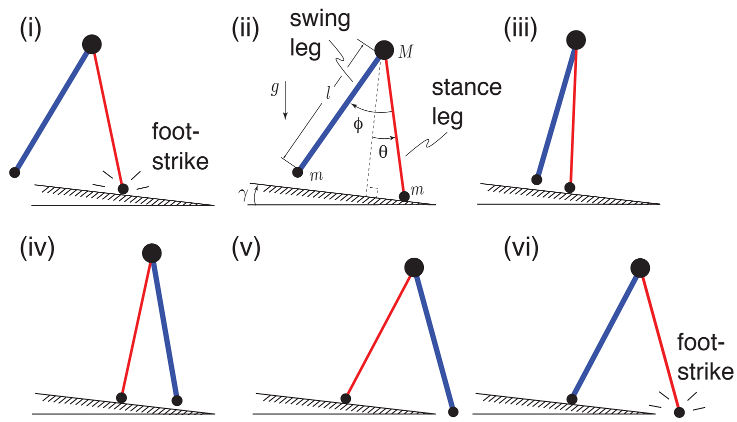

Figure 1.2: A typical step of the simplest walker.

A single step of the walker consists of the following sequence:

$$\underbrace{\text{Single Stance phase} \longrightarrow \text{Foot-ground contact event} \longrightarrow \text{Foot-strike phase} \longrightarrow}_{\text{one step/ period-one limit cycle}} \text{Single Stance} \tag{1.1}$$

Next, we state the equations of motion for the phases and events described in Eq. 1.1 and provide a brief explanation on the derivation. Please see the appendix for more details on the derivation.

Single stance phase (continuous dynamics):

In this phase of motion, the stance leg pivots and rotates about the stationary foot, while the swing leg pivots and rotates about the hinge connecting the two legs. The assumptions are: the stance leg does not slip, there is no hinge friction, and foot scuffing is ignored. The equations for this phase are

$$\ddot{\theta} = \sin(\theta - \gamma), \tag{1.2}$$

$$\ddot{\phi} = \sin(\theta - \gamma) + \{\dot{\theta}^2 - \cos(\theta - \gamma)\}\sin(\phi). \tag{1.3}$$

The Eq. (1.2) and Eq. (1.3) are obtained by doing an angular momentum balance about stance foot contact point and hip hinge respectively, followed by non-dimensionalizing the time with $\sqrt{\ell/g}$ and applying the limit, $m/M \to 0$.

Foot-ground contact event:

The swing leg contacts the ground when the following condition is met,

$$\phi = 2\theta. \tag{1.4}$$

Foot-strike phase (discontinuous dynamics):

In this phase of motion, the legs exchange their roles. That is, the current swing leg becomes the new stance leg and the current stance leg becomes the new swing leg. The assumptions are: the swing leg has a plastic collision (no slip and no bounce) with the ground, the collision is instantaneous, and there is no double support phase. The equations for this phase are:

$$\theta^+ = -\theta^-, \tag{1.5}$$
$$\phi^+ = -\phi^- = -2\theta^-, \tag{1.6}$$
$$\dot{\theta}^+ = \cos(2\theta^-)\dot{\theta}^-, \tag{1.7}$$
$$\dot{\phi}^+ = \Big(1 - \cos(2\theta^-)\Big)\cos(2\theta^-)\dot{\theta}^-, \tag{1.8}$$

where the super-script $-$ and $+$ denotes the instance just before and just after foot-strike respectively. The switching of the leg angles is given by Eq. (1.5) and Eq. (1.6). The angular rates of the legs after foot-strike are obtained by using conservation of angular momentum about the impending foot-strike point and the hinge joint at the hip to obtain Eq. (1.7) and Eq. (1.8) respectively. Then, time is non-dimensionalized using $\sqrt{\ell/g}$ and the limit, $m/M \to 0$, is applied.

1.3.2 Analysis using Poincaré return map

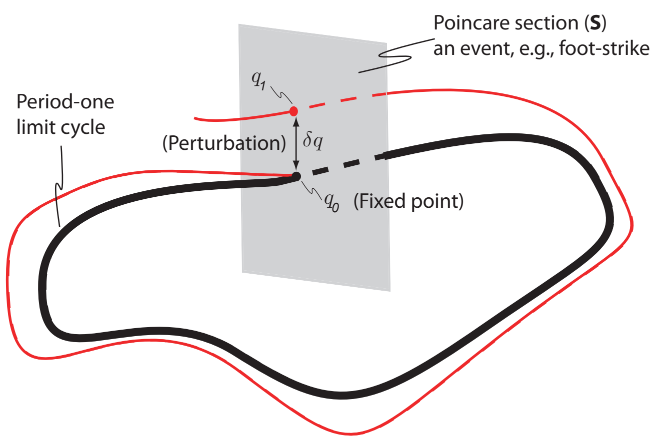

Figure 1.3: A Poincaré Map is used to find walking solutions and to analyze stability.

A Poincaré return map is used to find steady-state walking motions and to analyze motion stability [22, 38, 47]. In Figure 1.3, the gray region is the Poincaré section and denotes an instance in the walking motion (e.g., before foot-strike, after foot-strike, mid-stance).

We assume the Poincaré section to be the instance just after foot-strike. Let $\mathbf{q_0} = \{\theta_0^+, \dot{\theta}_0^+, \phi_0^+, \dot{\phi}_0^+\}$ be the state after foot-strike. Then, there is a function $\mathbf{S}$ that takes the initial condition, $\mathbf{q_0}$, and returns the state after one step, $\mathbf{q_1}$. The function $\mathbf{S}$ is called the stride map. Thus, the Poincaré map is, $\mathbf{q_1} = \mathbf{S}(\mathbf{q_0})$. There is an initial condition $\mathbf{q_0}$ such that

$$\mathbf{q_0} = \mathbf{S}(\mathbf{q_0}). \tag{1.9}$$

The above condition defines a period-one limit cycle. In other words, the initial condition after foot-strike,

Variable	Stable solution	Unstable solution
State, $\mathbf{q_0}$	$\begin{bmatrix} 0.200310900544287 \\ -0.199832473004977 \\ 0.400621801088574 \\ -0.015822999948318 \end{bmatrix}$	$\begin{bmatrix} 0.193937369810184 \\ -0.203866927442010 \\ 0.387874739620369 \\ -0.015144260853192 \end{bmatrix}$
Eigenvalues, λ	$\begin{bmatrix} 0 \\ 0.000000001586465 \\ -0.190099639402167 - i0.557599274284362 \\ -0.190099639402167 + i0.557599274284362 \end{bmatrix}$	$\begin{bmatrix} -0.000000000000002 \\ -0.000000005231481 \\ 0.459589047035257 \\ 4.003865226079296 \end{bmatrix}$

Table 1.1: Fixed points (first row and denoted by $\mathbf{q_0}$), eigenvalues using central difference (second row and denoted by λ), for the simplest walker for slope, $\gamma = 0.009$. The fixed points are accurate to 12 decimal places. The eigenvalues computed by central difference and with perturbation size of 10^{-5} and are accurate to 5 decimal places.

$\mathbf{q_0}$, defines a walker state that maps onto itself after one step. Similarly, one can find a period-two limit cycle by applying the function S twice and so on.

In general, it is not possible to find $\mathbf{S}$ and the state $\mathbf{q_0}$ analytically, so one needs to resort to numerical techniques. To compute $\mathbf{S}$, we first integrate the equations of motion in the single stance phase (Eq. (1.2) and Eq. (1.3)) till the foot-strike event (Eq. (1.4)), and apply the leg support exchange conditions (Eq. (1.5)-(1.8)). Finally, to find four initial conditions in $\mathbf{q_0}$, the zeros of Eq. 1.9 ($\mathbf{q_0} - \mathbf{S}(\mathbf{q_0}) = 0$) are found. The zeros can be found by root finding techniques such as Newton-Raphson's method. In our experience, a good initial guess is of paramount importance for the root finder to give quick results. To find good initial conditions, we recommend simulating and animating a single step to see if it is close to repeating and then use those as a guess for the root finder (also see [51]).

After obtaining $\mathbf{q_0}$, the stability of the period-one limit cycle is analyzed. To do this, one needs to compute the eigenvalues of Jacobian of the Poincaré map, $\mathbf{S}$. To obtain the Jacobian, we used the central difference with a step size of 10^{-5}. The limit cycle is stable if the magnitude of the biggest eigenvalue is less than 1 and unstable otherwise [22, 38, 47].

We give benchmark results for a ramp slope, $\gamma = 0.009$, the only free parameter in this model. Using the method described above, there are two period-one limit cycles. Tab. 1.1, first row, gives the two limit cycles. Table 1.1, second row, gives the eigenvalues of each of the fixed points, $\mathbf{q_0}$. As seen from the table, the middle column is the stable limit cycle because the biggest eigenvalue is inside the unit circle while the third column from left is the unstable limit cycle because the biggest eigenvalue is outside the unit circle. Thus one limit cycle is stable and the other is unstable. Figure 1.4 shows the angular position of the stance and swing leg as a function of time for the stable limit cycle and phase portrait of the stable limit cycle.

1.3.3 Passive dynamic walking in 3-dimensions

McGeer [39] and Garcia [23] analyzed a 3-D model with four degrees of freedom (roll or side-to-side, pitch or front-back, yaw or turning on the stance leg and inter-leg pitch angle between stance and swing leg). However, both of them were unable to find a stable walking gait. Kuo [33] considered a simpler 3D model without the yaw degree of freedom. After doing an exhaustive search, he found that one eigenvalue was always greater than one. This eigenvalue associated with this unstable gait was in the roll direction and was due to a mismatch in the roll velocity at ground contact condition. Further, he demonstrated that

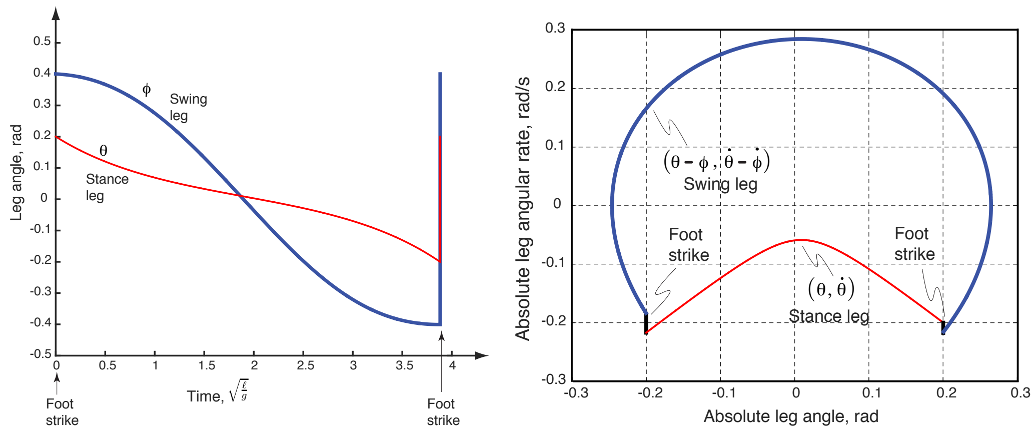

Figure 1.4: Left: Stance leg and swing leg angle as a function of time for one step of the simplest walker, Right: Phase portrait for one step of the simplest walker for slope, $\gamma = 0.009$.

several simple strategies such as: applying a torque in the yaw direction, spinning a reaction wheel, moving the upper body slightly, and controlling the lateral foot placement, all have the effect of stabilizing the roll motion while preserving the passive dynamics.

Collins et al. [17] were able to create a stable, 3D passive dynamic machine by adding swinging arms (see Fig. 1.1). Coleman and Ruina [14] created a non-anthropomorphic walker with ellipsoidal feet that was able to walk stably downhill. Though Coleman and Ruina were able to explain the stability of their walker using Poincaré based methods [13], it is not clear what design parameters are critical in achieving stable three-dimensional passive dynamic walking.

1.4 Powered bipedal robots inspired from passive dynamics

In walking robots, energy is lost each time the foot hits the ground (unless special mechanism is used to prevent collisional losses). In order to sustain steady walking, this energy needs to be supplied through external means. In case of passive dynamic robots walking downhill, this energy is supplied by gravity. These facts suggests two different approaches to enable level ground walking; (1) prevent energy loss during collision by suitable robot design (see Sec. 1.4.1), and (2) use an actuator to supply the lost energy (see Sec. 1.4.2). The rest of this section will highlight some of the methods to enable almost-passive walking on level ground.

1.4.1 Collisionless walking

One way to enable level ground walking with passive models is to find means of reducing the collisional losses at foot-strike to zero. Gomes and Ruina [24] created a passive dynamic walking model which had an upper-body that was coupled to each leg through a torsional spring (see Fig. 1.5 (a)). They found internal oscillatory modes of the upper body that ensures that the swing leg contacts the ground with zero velocity. Thus, the robot is able to sustain walking on level ground without external energy input. However, note that

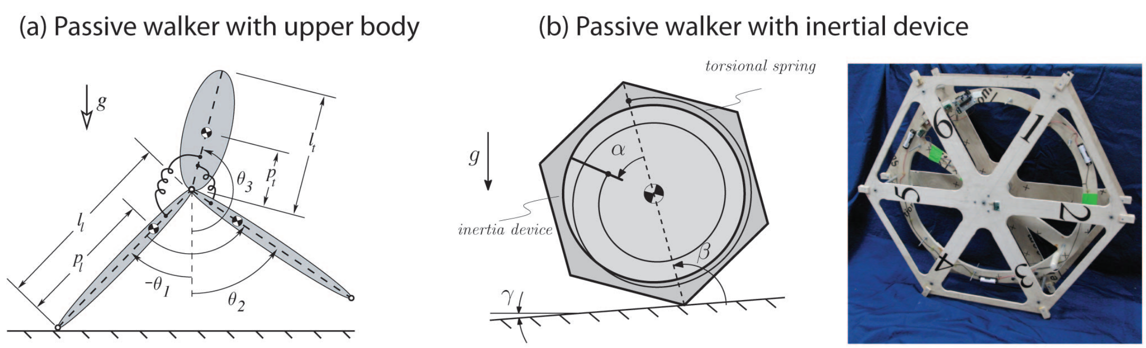

Figure 1.5: Collisionless walking models: (a) Bipedal walking model with upper body coupled to the legs through torsional springs [24], (b) Rimless walking model with inertial device with torsionally coupled spring [25].

the motion of the robot is unstable because even the slightest perturbation will create a collisional loss at foot-strike and the robot will be off the limit cycle. Thus there are no stable (asymptotic, uniform, etc.) solutions for collisionless locomotion models. Also, the model requires the swing foot to stick to the ground and later release for swing. Gomes and Ahlin [25] have created a physical prototype of a rimless wheel, another passive dynamic model [38], that can demonstrate nearly collision-less walking. Their device consists of the rimless wheel coupled to an inertial wheel through a torsional spring. Between the middle to the end of a step, the torsional spring transfers the energy of the rimless wheel to the inertial wheel thereby reducing the wheel velocity to almost zero just before the next spoke makes contact with the ground. The torsional spring then transfers the stored energy back to the wheel from start to the middle of the step speeding up the rimless wheel. This energy transfer ensures walking on level ground without collisional losses.

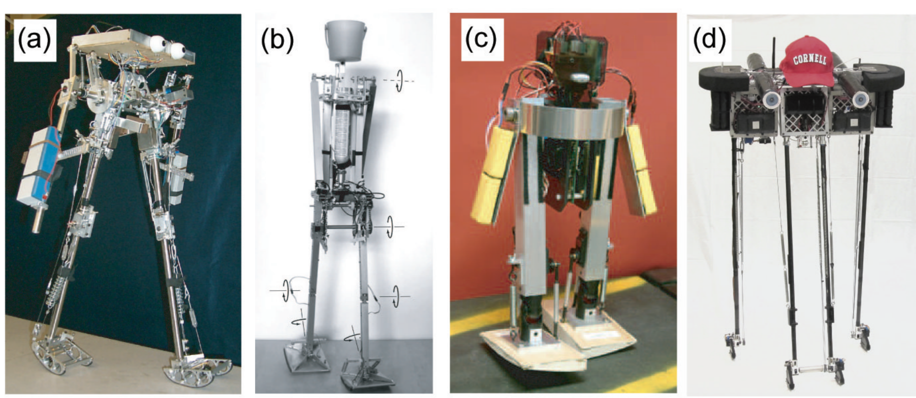

Figure 1.6: Powered walkers inspired from passive dynamics. (a) Cornell powered biped, (b) Delft powered biped, and (c) MIT learning biped. These figures are from [15], and (d) Cornell Ranger [7].

1.4.2 Actuating passive dynamic walking robots

In robots where collision-less walking is not possible, one can add one or more actuators to enable level ground walking. Figure 1.6 shows powered bipedal robots based on passive dynamic walking principles. The Cornell biped (Fig. 1.6 (a)) has five internal degrees of freedom (two ankles, two knees, and a hip), the arms are mechanically linked to the opposite leg, and the upper body is kinematically constrained so that its midline bisects the hip angle through a hip bisection mechanism. The robot is electrically powered by an ankle push-off that is triggered when the opposing foot hits the ground. The Delft biped (Fig. 1.6 (b)) is similar to Cornell biped, but is powered by pneumatic hip actuation and has a passive ankle. The MIT learning biped (Fig. 1.6 (c)) is based on the simpler ramp-walker passive hip, is powered by two servo motors in each ankle, and uses reinforcement learning to automatically acquire the controller [15]. The Cornell Ranger (Fig. 1.6 (d)) has three internal degrees of freedom (one hip and two ankles) and is electrically powered. More details on control of Ranger are discussed later in this section. Next, we review control schemes that preserve the natural dynamics while enabling walking on level ground.

Virtual passive dynamic walking is able to recreate downhill walking by adding a virtual gravity field using ankle and hip actuators. In passive dynamics walking with a downhill slope of γ, gravity makes an angle of γ with the direction perpendicular to the ramp. Thus, the component of gravity normal to the ramp is $g\cos(\gamma)$ and along the ramp is $g\sin(\gamma)$. But since γ is relatively small, one can approximate the normal component as g and horizontal component as $g\gamma$. However, if the slope was zero (level ground walking), then the component normal to the ground would be g and it would be 0 in the horizontal direction. From the above arguments we see that the walker on level ground is missing a horizontal component of $g\gamma$. Thus, the idea behind virtual passive dynamic walking control is to *use actuators* to create a virtual gravitational field such that the horizontal component is $g\gamma$ and leave the vertical component unaffected [1]. The resulting motion is very similar to passive dynamic walking on slope γ but it is on level ground. However, this requires both, an ankle as well as a hip actuator.

Another way to achieve almost passive dynamic walking is to track a constant mechanical energy. The key idea is that passive dynamic robots are able to maintain a periodic walking motions because their mechanical energy (i.e., kinetic + potential energy) is constant between steps. Thus to recreate passive dynamic walking on level ground, one can use the actuators to track this mechanical energy [26]. Further, each slope has a different total mechanical energy. Thus, by tracking the total mechanical energy for a given slope, the walking motion can be made slope independent. A key point here is that the tracking gains need to be kept low to ensure that the natural dynamics of the passive gait is preserved.

Yet another way of preserving passive dynamic walking is to use ON-OFF or bang-bang control to supply the energy lost during collision. Camp [12] presented a 2-D knee-less model with two legs and two powered ankles that used such an actuation scheme. The ankle motor is turned ON when the swing leg reaches a prescribed angle and shut-off at the instance of foot-strike. The walker exhibits a variety of stable and unstable limit cycles as the motor stall torque is varied. The stall torque is thus analogous to the ramp of the passive dynamic walker. An extreme case of this type of control is to use an impulse type control to power walking [20]. An impulse is provided at the beginning of the swing phase and no actuation is provided for the rest of the step. By choosing appropriate impulse at the beginning of swing phase the robot is able to walk stably.

Low gain Proportional-Derivative (PD) controllers can be used to create passive-dynamic like walking gaits on level ground. Typical implementation involves dividing the walking step into set of states or a state machine, and having different PD controllers and set-points for different states [11, 18]. The gains on the PD controller are weak so that they do not interfere with the natural dynamics of the legs.

Instead of using continuous feedback to track the mechanical energy, one can use feedback at discrete times in the walking step. For instance, when a passive dynamic robot walks on level ground without any control whatsoever, the end-of-step state will be different from the start-of-step state because of the collisional losses. The error can be used to derive feedback control law that nullifies the difference [40]. This type of control is called once per step control because the feedback error and corrections are based on sampling the state once per step. Bhounsule et al. [7] took a similar approach to stabilize the robot Ranger (see Fig. 1.6(d)) which walked a distance of 40.5 miles non-stop on a single battery charge. The stabilization is in addition to the energy-optimal trajectory controller that is set up on the robot. The Poincaré map for Ranger is about the mid-stance position. The energy-optimal trajectory is linearized about the Poincaré map. In the linearized equations, the state variables are the stance leg velocity, swing leg position and velocity at mid-stance and the control actions are the foot placement and ankle push-off. The linearized equations are used to set up a discrete linear quadratic regulator to reduce the errors in the state at the Poincaré section [8]. We provide more details in the next section.

1.4.3 Discrete-decision continuous action control

Next, we present a controller formulation that does discrete, event-based, intermittent control that is able to preserve much of the passive dynamics of walking robots (also see [8]). We illustrate the problem with a hypothetical example and then show how it can be used to control a bipedal robot.

Control problem

Let the state of the full, possibly non-linear, system be $x(t)$, the control be $u(t)$ and the continuous system dynamics defined by F with $\dot{x} = F(x, u)$. Further, assume the system has a desirable nominal trajectory $\bar{x}(t)$ associated with a nominal baseline control $\bar{u}(t)$:

$$\dot{\bar{x}} = F(\bar{x}, \bar{u}). \tag{1.10}$$

The feedforward command $\bar{u}(t)$ in the above equation is open loop and does not stabilize the system adequately, or perhaps at all. For example, even with perfect initial conditions, modeling errors, actuator imperfections and disturbances will cause the system to too-much, or catastrophically ('failure'), deviate from the nominal trajectory. So we add a feedback control that supplements u with a control δu to adequately brings the system back to the nominal trajectory. In this case, we do feedback at discrete times and the control commands are simple feedforward control functions over the interval. This differs from common continuous feedback control because we only sense key quantities and only at occasional times.

Schematic example

We illustrate the event-based intermittent feedback control idea with a schematic example. Consider the nominal trajectory of a second-order system shown as a solid red color line in Fig. 1.7. Let n and $n+1$ be instances of time at which we are taking measurements from sensors. The time interval between the measurements n and $n+1$ is typically on the order of the characteristic time scale of interest (and *not* the shortest time our computational speed allows). Let us assume that we take two measurements, $x_n = [x_1 \quad x_2]'$ (e.g., a position and velocity) at time n. We want to regulate two outputs: z_1 and z_2 (some attributes of the state x_n) at time $n+1$.

Assume that, due to external disturbances, the system has deviated from its nominal trajectory. We show the trajectory as a dashed blue color line in Fig. 1.7 (a). Now, the state of the system is $\bar{x}_n$ ($\neq x_n$) at time n. When feedback corrections are absent, the relevant output $\bar{z}_{n+1}$ ($\neq z_{n+1}$) whose components, in notational shorthand, are $[\bar{z}_1 \quad \bar{z}_2]'$.

Our feedback controller measures deviations at time n ($\delta x_n = x_n - \bar{x}_n$) and uses actuation to reduce the deviations in output variables ($\delta z_{n+1} = z_{n+1} - \bar{z}_{n+1}$). For illustration, we choose two control actions,

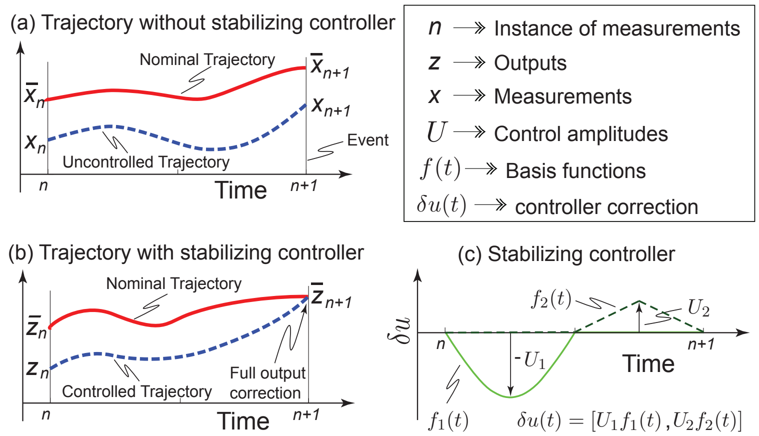

Figure 1.7: Schematic example. (a) Shows the nominal (solid red) and deviated (dashed blue) trajectory, for some dynamic variable x of interest. We measure the state x at the start of a continuous interval, namely at section n. (b) Shows the new deviated trajectory in target variables z after switching on our feedback controller. In this example, feedback controller nulls (zeros) the output z at the end of the interval, illustrating a ‘dead-beat’ controller. (c) The feedback motor program has two control actions: a sinusoid for first half cycle and a hat function for the second half of the cycle. These shapes are arbitrary and different from each other in form only for illustrative purposes. They could overlap in time. We choose the amplitudes U_1 and U_2 of the two functions at the start of the interval depending on the error $(x - \bar{x})$. By a proper choice of the amplitudes U_1 and U_2 deviations are, in this example, fully corrected in between measurements. The choice of trigger for event n, the choice of sensor measurements x, the choice of output variables z, and the control shape functions $f(t)$ are offline design choices.

$\delta\mathbf{u}_n = [U_1 f_1(t) \;\; U_2 f_2(t)]'$, a half sinusoid and a hat function, each active for half the time between time $n+1$ and n (Fig. 1.7 (c)). The controller adjusts the amplitudes (U_1 and U_2) of the two control functions, based on measured deviations δx_n, to regulate the deviated outputs δz_{n+1}. For example, with a proper choice of the amplitudes, it should be possible to fully correct the deviations in the output variables, as seen in Fig. 1.7 (b).

In the simplest cases, we linearize the map from the measurement section n to the section $n+1$. The sensitivities of the dynamic state to the previous state and the controls $\mathbf{U}_n = [U_1 \;\; U_2]'$ are: $\mathbf{A} = \partial x_{n+1}/\partial x_n$, $\mathbf{B} = \partial x_{n+1}/\partial \mathbf{U}_n$, $\mathbf{C} = \partial z_{n+1}/\partial x_n$ and $\mathbf{D} = \partial z_{n+1}/\partial \mathbf{U}_n$. The brute-force way of calculating the sensitivity matrices $\mathbf{A}, \mathbf{B}, \mathbf{C}$ and $\mathbf{D}$ is by numerical finite-difference calculations. We then have, for our linearized discrete system model:

$$\delta x_{n+1} = \mathbf{A}\delta x_n + \mathbf{B}\mathbf{U}_n \tag{1.11}$$

$$\delta z_{n+1} = \mathbf{C}\delta x_n + \mathbf{D}\mathbf{U}_n. \tag{1.12}$$

Again, the δx_n are a list of measured deviations, the δz_n are a list of deviations which we wish to control, the $\mathbf{U}$ are the activation amplitudes (2 in our example above). For simplicity, assume full state measurement, the controller architecture is thus

$$\mathbf{U}_n = -\mathbf{K}\delta x_n, \tag{1.13}$$

where $\mathbf{K}$ is a constant gain matrix. We choose the gains $\mathbf{K}$ to meet or optimize various goals using a discrete linear quadratic regulator (DLQR).

For most systems, ones that have the needed controllability, it is possible to find shape functions $f_1(t)$ and $f_2(t)$ so that the matrix $\mathbf{B}$ is non-singular. In the same way that a square matrix is generically non-singular, n random shape functions for an n order system should (generically) lead to a non-singular $\mathbf{B}$ and thus the possibility of 1-step dead-beat control. Of course the matrix $\mathbf{B}$ can be more or less well conditioned depending on how independent the shape functions are from each other.

Discrete linear quadratic regulator (DLQR)

One can use a DLQR to any goal function z of the state. In DLQR [43], we seek to minimize the cost function J_{dlqr} defined as,

$$J_{\text{dlqr}} = \sum_{n=0}^{n=\infty} \left(\delta z_{n+1}{}^T \mathbf{Q}_{zz} \delta z_{n+1} + \mathbf{U}_n{}^T \mathbf{R}_{UU} \mathbf{U}_n \right), \tag{1.14}$$

where $\mathbf{Q}_{zz}$ and $\mathbf{R}_{UU}$ are matrices that weight the different components of δz_{n+1} and $\mathbf{U}_n$ ($\mathbf{R}_{UU}$ must be positive definite and $\mathbf{Q}_{zz}$ positive semi-definite). The weights $\mathbf{Q}_{zz}$ and $\mathbf{R}_{UU}$ are design parameters picked to give reasonably fast return to nominal values but without unduly high gains (which might tend to lead to control command that are beyond safety limits). They are often given as diagonal for simplicity.

Putting Eqn. (1.12) in Eqn. (1.14) and re-arranging gives,

$$J_{\text{dlqr}} = \sum_{n=0}^{n=\infty} \left(\delta x_n{}^T \mathbf{Q} \delta x_n + 2\delta x_n{}^T \mathbf{N} \mathbf{U}_n + U_n{}^T \mathbf{R} \mathbf{U}_n \right), \tag{1.15}$$

where $\mathbf{Q} = \mathbf{C}^T \mathbf{Q}_{zz} \mathbf{C}$, $\mathbf{N} = \mathbf{D}^T \mathbf{Q}_{zz} \mathbf{C}$ and $\mathbf{R} = \mathbf{D}^T \mathbf{R}_{zz} \mathbf{D} + \mathbf{R}_{UU}$. J_{dlqr} can be minimized with a linear state feedback, $\mathbf{U}_n = -\mathbf{K}\delta x_n$ with gain $\mathbf{K}$ found by solving the standard Ricatti equation [43].

Other goals.

The same linear control architecture given by Eqn. 1.13, could have gains $\mathbf{K}$ chosen to optimize or achieve other criteria that do not fit into standard basic linear control formalisms. For example, there could be a weight on the sparseness of $\mathbf{K}$, on non-quadratic costs for error and control over some range of initial conditions, on the basin of attraction for the non-linear system, etc. To calculate $\mathbf{K}$ one might then require more involved optimization calculations, but the structure of the resultant controller would be preserved. Similarly the choice of shape functions could be subject to optimization on independence, smoothness, maximizing control authority, etc.

Factors to consider while designing the controller:

The systems we are interested in controlling are not those in which we do measure control quality by how closely a target is followed, clearly the type of intermittent control we discuss here is not optimal for that. Rather, we are interested in preventing total system failure. For walking or for an inverted pendulum, falling down is failure. To slightly generalize, by failure we mean that the system state has moved outside a particular target region surrounding the target point. How is this region defined? In practice, it is the region outside of which non-linear effects lead to divergence of the solution to points much farther from the target (e.g., falling down). Sticking to the linear model, the user has to supply the target region based on intuitions, experience, or non-linear modeling. Some issues in the controller design include:

1. Selecting a suitable section or instance of time to take measurements — this instant should be when the dynamic-state estimation is reasonably accurate, and when dynamic-state errors which cause failure are evident;

2. selecting measurement variables (x_n) that are well-predict system failure;

3. picking output variables (z_n) that can well-correct against system failure; and

4. picking actuator shape profiles ($f(t)$'s) that have large, and relatively independent, effects on the target variables, and are also sufficiently smooth for implementation with real motors.

We next discuss the above points with in the context of a walking robot.

Example: Controlling a bipedal walking robot

For a 2D bipedal robot walking at steady speed, here is how we can go about designing a discrete controller [5]. A typical walking step of a bipedal robots includes two phases: a smooth continuous phase in which the entire robot vaults over the grounded leg, and a non-smooth discontinuous phase in which the legs exchange roles.

1. Suitable section or instance of time to take measurements: Any instant not-close to support-exchange is a good time for measurement. This is because the measurements are typically noisy during the non-smooth support change (heel-strike collision).

2. Suitable measurement variables (x_n) that are representative of system failure: The state of the lower body is most important for walking balance, so good measurement variables are the state (position and velocity) of the stance leg.

3. Suitable output variables (z_n) that also correlate with system failure: Step time, step length are important quantities to regulate during walking, and they serve as good output variables.

4. Suitable actuator shape profiles ($f(t)$'s) that have large and relatively independent effects on the target variables: For leg swing, for example, two torque profiles, one with large amplitude near the start of the interval, and one with large amplitude near the end, yield good control authority over position and velocity of the swing leg at the end of the interval.

Once the above quantities are picked, we can check the system controllability. If the system is not well controllable (correction of reasonable disturbances requires unreasonable actuation amplitudes) the first likely fix is picking better actuation shape functions.

As noted, we used this discrete feedback control idea to stabilize steady walking gait of a bipedal robot leading to energy-efficiency record and long distance 65 km walking record [7, 9, 45].

Computing the linearization

For linear control approaches, the gain selection depends on having the linearized map Eqn. (1.11) and Eqn. (1.12) from Eqn. (1.10). We assume we have a system, or computational model of the system, with which we can perform numerical experiments. To get the matrices $\mathbf{A}$ and $\mathbf{C}$, we can perturb x_n element-wise and use finite difference to compute these matrices. Similarly to get matrices $\mathbf{B}$ and $\mathbf{D}$, we can put in small amplitudes of the controls $\mathbf{U}_n$ and use finite difference to compute the sensitivities.

1.5 Discussion and Challenges

Energy efficiency and Dynamic Walking

Energy-efficiency for a variety of locomotion/mobility modes is quantified by Total Cost Of Transport (TCOT) [48] and the Mechanical Cost Of Transport (MCOT) which are defined as follows,

$$\text{TCOT} = \frac{\text{Total Energy used per step}}{\text{weight} \times \text{step length}}, \tag{1.16}$$

$$\text{MCOT} = \frac{\text{Mechanical Energy used per step}}{\text{weight} \times \text{step length}} \tag{1.17}$$

The total energy includes the mechanical energy and other energy-terms like dissipation in the resistive elements of electric motors, energy to power the electronics (e.g., sensors, computers). For passive dynamic walkers, the total energy is equal to the mechanical energy and is equal to the tangent of the ramp slope. Thus, MCOT = $\tan(\gamma)$ = TCOT, where γ is the ramp slope. McGeer's Dynamite had a TCOT = MCOT = 0.025 [38]. Some of the most energy-efficient powered legged robots are: Collins biped (TCOT = 0.2, MCOT = 0.055 [16]; Cornell Ranger (TCOT = 0.19, MCOT = 0.04) [7]; and Cargo (TCOT = 0.1) [28]. To put these numbers in perspective, humans have a TCOT = 0.3 [2] [1] and MCOT = 0.05 [37]. Note that both, TCOT and MCOT are a function of the step size and step velocity and the above values correspond to the lowest energy values at a specific step size and step velocity [4].

Stability and Robustness

Passive dynamic-based walkers have shown poor stability and robustness characteristics. The most well-known method of computing stability of passive dynamic-based robots is using the eigenvalues of the limit cycle (see Sec. 1.3.2). The walking motion is stable if the magnitude of the biggest eigenvalue is less than 1 and unstable otherwise. In particular, an eigenvalue equal to 0 implies that all disturbances are nullified in a single step. Thus a values closer to zero implies greater stability. However, passive dynamic robots have rarely demonstrated an eigenvalue less than $0.6 > 0$ [7]. One way of stabilizing the passive dynamic-based walkers is to develop a controller that sets the eigenvalue to a desired value, also known as pole placement [7, 8, 33]. Another option is to minimize the biggest eigenvalue during the controller design phase [42].

A commonly used metric for robustness of passive dynamics-based walkers is the maximum change in height that the robot can withstand without falling [52]. One can non-dimensionalize the change in height with the leg length to compare different robots. The maximum step-down (normalized by leg length) for passive dynamics-based robots from TU Delft are: Max, 1%, Denise 1%, and Mike 2% [29], indicating poor robustness to terrain variation. Kim and Collins [32] have found that adding random disturbances rather than a single disturbance is a better indicator of stability. They have also found that to get consistent results, one needs to evaluate stability (ability to not fall) over 100 steps. Kelly and Ruina [31] provide a technique for creating asymptotically stable and robust using Lyapunov function. But all the approaches so far, evaluate the robustness after controller design. A challenge then, is to come up with a technique to design a controller for a given robustness.

Versatility, Maneuverability, Agility

Versatility refers to the ability of the bipedal robot to stand, walk, turn, and climb stairs [35]. Maneuverability is the robot's ability to turn its body or change the heading [21, 30] and agility is defined as the robot's ability to change its velocity [10]. Passive dynamics-based robots have demonstrated very limited

[1] The TCOT is computed using the total metabolic energy.. However, if only the energy to walk is taken into account then human TCOT is 0.2.

versatility, agility, and maneuverability. There does not seem to be any fundamental limitation in addressing these metrics except that very limited work has been done in this regard.

Mechanical Design

Proper tuning of the mass distribution, inertia, and leg geometry is vital to enable un-actuated passive dynamic walking down a ramp. We discuss the issues next.

The natural frequency of the swinging leg should be such that it is able to swing forward to break the forward fall about the stance leg. The natural frequency depends on the leg inertia and the location of the center of mass of the leg. The pendulum swing time is directly proportional to the inertia of the leg and inversely proportional to the location of the center of mass of the leg. Thus, by increasing the inertia or moving the center of mass near the torso increases the swing time and which increases the natural frequency of walking. If the natural frequency increases too much then there will be no passive walking solutions. However, moving the center of mass away from the pin joint will increase the energy loss at foot-strike leading to energy-inefficiency. Thus, there is a tradeoff in locating the center of mass on the legs. Another key parameter is the offset of the center of mass with respect to the line joining the hip joint and the foot contact point. Simulations have shown that the existence of walking solutions are extremely sensitive to the mass fore-aft offset.

Adding an upper body increases the energy-efficiency and stability of a 2D model of walking but adds more complexity to the walker [50]. One way of reducing the complexity is to kinematically couple the upper body to the legs through a hip bisection mechanism. The hip bisection mechanism ensures that the angle of the upper body is the average of the angle between the two legs. However, it is conjectured that the hip bisection mechanism could potentially reduce the energy efficiency because of the need to actively counteract effects of the torso on the trailing leg following collision (private communication, Steve Collins).

A circular shaped foot is more energy-efficient than a point foot. As the radius of curvature of the foot increases, the collisional losses at foot-strike decreases, thereby increasing energy-efficiency. When the radius of curvature of the foot is equal to the leg length, there is a collision free support transfer between the legs, provided the center of mass is also at the hip joint. Such a walker is called a synthetic wheel [38] and can walk on level ground without using external energy.

Walking robots also need a mechanism that will enable ground clearance during leg swing. One technique is to use sideways rocking to allow for ground clearance (e.g., see Wilson Walker, Fig. 1.1 (a)) . To enable rocking, the bottom of the feet are made circular in the longitudinal as well as lateral direction with the center of both arcs approximately at the same place [33]. In addition, the leg mass, center of mass, and inertia needs to be tuned so that the lateral and longitudinal swing leg motion have the correct frequency which is dependent on the slope and dynamics of the rest of the walker. Another technique of creating ground clearance is to use knees but needs proper design (e.g., a latching mechanism) to prevent knee buckling. As both these methods add additional degrees of freedom, it also decreases the range of passive walking solutions.

Finally, friction in joints need to be as little as possible. Simulations with passive dynamic walkers have shown that passive dynamic walking solutions disappear as the friction increases [38]. For a passive inspired powered robot it is vital for the motors to be back-drivable to allow for passive leg swing.

Estimation

Good control depends on good estimates of the robot state and perhaps of the external disturbances. For example, to create energy-efficient walking with ankle actuation, the timing of push-off is critical. Push-off before heel-strike is four times cheaper than push-off after heel-strike [34, 46]. However, to do push-off just before heel-strike one needs good estimates of the time to heel-strike, which depends on the stance and swing leg angles and the terrain. Since it is next to impossible to have a precise estimate of all these things, it is not possible to determine the exact time to heel-strike. A compromise is to start the rear ankle push-off as the front foot hits the ground so as to achieve an overlap between the two. Sometimes it might be necessary to know the robot state just after heel-strike (e.g., if control is based on instance after heel-strike). However, the robot is vibrating at the instance after heel-strike which makes it challenging to do state estimation. Finally, almost all passive dynamic robots walk blindly. If these robots have to walk in practical scenarios such as in the presence of obstacles or stepping stones, it is crucial to incorporate vision based estimation and modify the control algorithm accordingly.

Higher dimensional systems

Most successful passive dynamics-based walkers have a few degrees of freedom, typically between 3 to 6. It is not obvious how to extend passive dynamics control approach to high dimensional systems such as humanoids which have 10+ degrees of freedom. Most humanoids are versatile but not quite energy-efficient (TCOT of Honda's ASIMO is around 3.2 and that of Boston Dynamics' PETMAN/ATLAS is around 5 [7]). Creating energy-efficient and versatile humanoids will dramatically increase their practicality.

1.6 Conclusion

Passive dynamic walking is an attractive concept because of the low energy usage and the naturalness in the motion. However, the major drawbacks of passive-dynamics robots are: limited robustness, limited versatility and limited agility/maneuverability which restricts their applications to simple systems and simple scenarios. How to create walking machines that meet all the above metrics is clearly an important, but unsolved challenge.

1.7 Acknowledgements

This work was partially supported by NSF grant number IIS-1566463.

1.8 Appendix

1.8.1 Derivation of equations of motion for the simplest walker

The equations of motion for the simplest walker were given in Section 1.3. We provide more details here.

Single stance phase

The equations of motion in single stance phase are given below:

$$\mathbf{A}_{\mathrm{SS}}\mathbf{X}_{\mathrm{SS}} = \mathbf{b}_{\mathrm{SS}} \tag{1.18}$$

$$\mathbf{A}_{\mathrm{SS}} = \begin{bmatrix} -\ell^2\ (M + 2\,m - 2\,m\,\cos(\phi)) & -\ell^2\,m\ (\cos(\phi) - 1) \\ l^2\,m\ (\cos(\phi) - 1) & \ell^2\,m \end{bmatrix}, \qquad \mathbf{X} = \begin{bmatrix} \ddot{\theta} \\ \ddot{\phi} \end{bmatrix},$$

$$\mathbf{b}_{\mathrm{SS}} = \begin{bmatrix} M\,g\,\ell\,\sin(\gamma - \theta) - \ell^2\,m\,\dot{\phi}^2\,\sin(\phi) - g\,\ell\,m\,\sin(\gamma - \theta + \phi) + g\,\ell\,m\,\sin(\gamma - \theta) + 2\,\ell^2\,m\,\dot{\theta}\,\dot{\phi}\,\sin(\phi) \\ \ell^2\,m\,\dot{\theta}^2\,\sin(\phi) - g\,\ell\,m\,\sin(\gamma - \theta + \phi) \end{bmatrix}$$

To reduce them to the simplest walker Equations 1.2 and 1.3, we non-dimensionalize time with $\sqrt{\ell/g}$ and take the limit $m/M \to 0$.

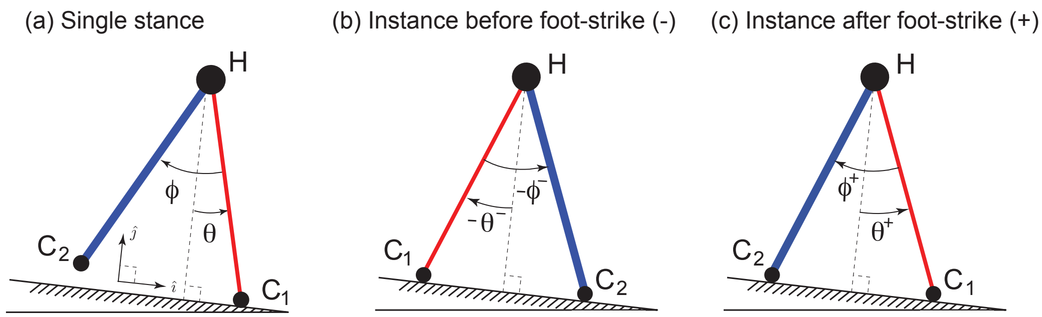

Figure 1.8: (a) Simplest walker in single stance phase. This caricature is used to derive equation for single stance mode. (b,c) Simplest walker at an instance just before and after foot-strike respectively. These two caricatures are used to relate angles and velocities after foot-strike with those before foot-strike.

Next, we give more details about the derivation of the equation for single stance. Let $\dot{\overrightarrow{H}}_{/X}$ and $\overrightarrow{M}_{/X}$ denote the rate of change of angular momentum and external torque about the point X, respectively. The first and second lines in the above equation are obtained by equating the angular momentum to the external torque about the foot in touch with the ground, C_1, and the hip, H, respectively. These points of interest are shown in Figure 1.8 (a). We obtain the following equations:

$$\dot{\overrightarrow{H}}_{/C_1} = \overrightarrow{M}_{/C_1}, \tag{1.19}$$

$$\dot{\overrightarrow{H}}_{/H} = \overrightarrow{M}_{/H} \, . \tag{1.20}$$

The above two equations can be written as:

$$\vec{r}_{H/C_1} \times M\,\vec{a}_H + \vec{r}_{C_2/C_1} \times m\,\vec{a}_{C_2} = \vec{r}_{H/C_1} \times M\,\vec{g} + \vec{r}_{C_2/C_1} \times m\,\vec{g}, \tag{1.21}$$

$$\vec{r}_{C_2/H} \times m\,\vec{a}_{C_2} = \vec{r}_{C_2/H} \times m\,\vec{g}, \tag{1.22}$$

where:

$$\vec{g} = g\,\hat{\jmath}\,\cos(\gamma) - g\,\hat{\imath}\,\sin(\gamma)\,, \tag{1.23}$$

$$\vec{a}_H = -\hat{\imath}\left(l\ddot{\theta}\,\cos(\theta) - l\dot{\theta}^2\,\sin(\theta)\right) - \hat{\jmath}\left(l\,\cos(\theta)\,\dot{\theta}^2 + l\ddot{\theta}\,\sin(\theta)\right), \tag{1.24}$$

$$\begin{aligned} \vec{a}_{C_2} = &-\hat{\imath}\left(l\ddot{\theta}\,\cos(\theta) - l\,\cos(\theta-\phi)\,\left(\ddot{\theta}-\ddot{\phi}\right) - l\dot{\theta}^2\,\sin(\theta) + l\,\sin(\theta-\phi)\,\left(\dot{\theta}-\dot{\phi}\right)^2\right)\ldots \\ &-\hat{\jmath}\left(l\ddot{\theta}\,\sin(\theta) + l\dot{\theta}^2\,\cos(\theta) - l\,\sin(\theta-\phi)\,\left(\ddot{\theta}-\ddot{\phi}\right) - l\,\cos(\theta-\phi)\,\left(\dot{\theta}-\dot{\phi}\right)^2\right), \end{aligned} \tag{1.25}$$

$$\vec{r}_{H/C_1} = \hat{\jmath}\,l\,\cos(\theta) - \hat{\imath}\,l\,\sin(\theta)\,, \tag{1.26}$$

$$\vec{r}_{C_2/C_1} = \hat{\jmath}\,(l\,\cos(\theta) - l\,\cos(\theta-\phi)) - \hat{\imath}\,(l\,\sin(\theta) - l\,\sin(\theta-\phi))\,, \tag{1.27}$$

$$\vec{r}_{C_2/H} = \hat{\imath}\,l\,\sin(\theta-\phi) - \hat{\jmath}\,l\,\cos(\theta-\phi)\,. \tag{1.28}$$

To create an actuated model, a hip torque and an ankle torque needs to be added to the first and second line of $\mathbf{b}_{\mathrm{SS}}$ in Eq. 1.18, respectively.

Foot-strike phase

The angles after foot-strike are obtained by comparing the angles in Figure 1.8 (b) with that in Figure 1.8 (c). These are given by:

$$\theta^+ = -\theta^-, \tag{1.29}$$
$$\phi^+ = -\phi^- = -2\theta^-. \tag{1.30}$$

The angular velocities after foot-strike are given by:

$$\mathbf{A}_{\text{hs}}\mathbf{X}_{\text{hs}} = \mathbf{b}_{\text{hs}}, \tag{1.31}$$
$$\mathbf{A}_{\text{hs}} = \begin{bmatrix} \ell^2\ (M + 2\,m - 2\,m\ \cos(\phi)) & \ell^2\,m\ (\cos(\phi) - 1) \\ -l^2\,m\ (\cos(\phi) - 1) & -\ell^2\,m \end{bmatrix}, \mathbf{X}_{\text{hs}} = \begin{bmatrix} \dot\theta^+ \\ \dot\phi^+ \end{bmatrix}, \mathbf{b}_{\text{hs}} = \begin{bmatrix} M\,\ell^2\,\dot\theta^-\ \cos(\phi^-) \\ 0 \end{bmatrix} \tag{1.32}$$

To reduce the above two equations to the simplest walker Equations 1.7 and 1.8, we non-dimensionalize time with $\sqrt{\ell/g}$ and take the limit $m/M \to 0$.

Next, we show how to obtain the above velocities after heel-strike. Let $\overrightarrow{H}^-_{/X}$ and $\overrightarrow{H}^+_{/X}$ denote the angular momentum about the point X before (superscript $-$) and after (superscript $+$) foot-strike respectively. The first and second lines in the above equation are obtained by equating the angular momentum about the foot that is about to touch the the ground, C_1, and the hip, H, respectively to get the following equations:

$$\overrightarrow{H}^-_{/C_2} = \overrightarrow{H}^+_{/C_1}, \tag{1.33}$$
$$\overrightarrow{H}^-_{/H} = \overrightarrow{H}^+_{/H}\ . \tag{1.34}$$
$$\tag{1.35}$$

Note that for the instance after foot-strike the contact points C_1 and C_2 are swapped. The above equation can be written as:

$$\vec{r}^{\,-}_{H/C_2} \times M\ \vec{v}^{\,-}_H + \vec{r}^{\,-}_{C_1/C_2} \times m\ \vec{v}^{\,-}_{C_1} = \vec{r}^{\,+}_{H/C_1} \times M\ \vec{v}^{\,+}_H + \vec{r}^{\,+}_{C_2/C_1} \times m\ \vec{v}^{\,+}_{C_2}, \tag{1.36}$$
$$\vec{r}^{\,-}_{C_1/H} \times m\ \vec{v}^{\,-}_{C_1} = \vec{r}^{\,+}_{C_2/H} \times m\ \vec{v}^{\,+}_{C_2}, \tag{1.37}$$

where:

$$\vec{r}^{\,-}_{H/C_2} = \hat{\jmath}\,\ell\,\cos(\theta^- - \phi^-) - \hat{\imath}\,\ell\,\sin(\theta^- - \phi^-)\,, \tag{1.38}$$

$$\vec{r}^{\,-}_{C_1/C_2} = \hat{\imath}\,(\ell\,\sin(\theta^-) - \ell\,\sin(\theta^- - \phi^-)) - \hat{\jmath}\,(\ell\,\cos(\theta^-) - \ell\,\cos(\theta^- - \phi^-))\,, \tag{1.39}$$

$$\vec{r}^{\,+}_{H/C_1} = \hat{\jmath}\,\ell\,\cos(\theta^+) - \hat{\imath}\,\ell\,\sin(\theta^+)\,, \tag{1.40}$$

$$\vec{r}^{\,+}_{C_2/C_1} = \hat{\jmath}\,(\ell\,\cos(\theta^+) - \ell\,\cos(\theta^+ - \phi^+)) - \hat{\imath}\,(\ell\,\sin(\theta^+) - \ell\,\sin(\theta^+ - \phi^+))\,, \tag{1.41}$$

$$\vec{r}^{\,-}_{C_1/H} = \hat{\imath}\,\ell\,\sin(\theta^-) - \hat{\jmath}\,\ell\,\cos(\theta^-)\,, \tag{1.42}$$

$$\vec{r}^{\,+}_{C_2/H} = \hat{\imath}\,\ell\,\sin(\theta^+ - \phi^+) - \hat{\jmath}\,\ell\,\cos(\theta^+ - \phi^+)\,, \tag{1.43}$$

$$\vec{v}^{\,-}_{H} = -\hat{\imath}\,\ell\,\dot{\theta}^-\,\cos(\theta^-) - \hat{\jmath}\,l\,\dot{\theta}^-\,\sin(\theta^-)\,, \tag{1.44}$$

$$\vec{v}^{\,-}_{C_1} = 0, \tag{1.45}$$

$$\vec{v}^{\,+}_{H} = -\hat{\imath}\,\ell\,\dot{\theta}^+\,\cos(\theta^+) - \hat{\jmath}\,\ell\,\dot{\theta}^+\,\sin(\theta^+)\,, \tag{1.46}$$

$$\vec{v}^{\,+}_{C_2} = \Big(-\hat{\imath}\,\big(l\,\dot{\theta}^-\,\cos(\theta^-) - \ell\,\cos(\theta^- - \phi^-)\big) - \hat{\jmath}\,\big(\ell\,\dot{\theta}^-\,\sin(\theta^-) - \ell\,\sin(\theta^- - \phi^-)\big)\Big)\big(\dot{\theta}^- - \dot{\phi}^-\big)\,. \tag{1.47}$$

Bibliography

[1] F. Asano, M. Yamakita, and K. Furuta. Virtual passive dynamic walking and energy-based control laws. In *Proc. of IEEE/RSJ International Conference on Intelligent Robots and Systems, Takamatsu, Japan*, volume 2, pages 1149–1154, 2000.

[2] E. Atzler, R. Herbst, G. Lehmann, and E. Muller. Arbeitsphysiologische studien. *Pflugers Archiv European Journal of Physiology*, 208(1):184–244, 1925.

[3] B.U. Bechstein. Improvements in and relating to toys, 1912. UK Patent 7453.

[4] J.E.A. Bertram and A. Ruina. Multiple walking speed–frequency relations are predicted by constrained optimization. *Journal of theoretical Biology*, 209(4):445–453, 2001.

[5] Pranav A. Bhounsule. Control of a compass gait walker based on energy regulation using ankle push-off and foot placement. *Robotica*, FirstView:1–11, 6 2014.

[6] Pranav A Bhounsule. Numerical accuracy of two benchmark models of walking: the rimless spoked wheel and the simplest walker. *Dynamics of Continuous, Discrete and Impulsive Systems, Series B: Applications and Algorithms*, page 137148, 2014.

[7] Pranav A Bhounsule, Jason Cortell, Anoop Grewal, Bram Hendriksen, JG Daniël Karssen, Chandana Paul, and Andy Ruina. Low-bandwidth reflex-based control for lower power walking: 65 km on a single battery charge. *The International Journal of Robotics Research*, 33(10):1305–1321, 2014.

[8] Pranav A Bhounsule, Andy Ruina, and Gregg Stiesberg. Discrete-decision continuous-actuation control: balance of an inverted pendulum and pumping a pendulum swing. *Journal of Dynamic Systems, Measurement, and Control*, 137(5):9, 2014.

[9] Pranav Audhut Bhounsule. *A controller design framework for bipedal robots: trajectory optimization and event-based stabilization*. PhD thesis, Cornell University, 2012.

[10] Alan Bowling. Impact forces and agility in legged robot locomotion. *Journal of Vibration and Control*, 17(3):335–346, 2011.

[11] D.J. Braun and M. Goldfarb. A controller for dynamic walking in bipedal robots. In *Proceedings of 2009 IEEE International Conference on Intelligent Robots, St. Louis, MO, USA*, 2009.

[12] J. Camp. Powered 'passive' dynamic walking. Master's thesis, Cornell University, 1997.

[13] Michael J Coleman, Mariano Garcia, Katja Mombaur, and Andy Ruina. Prediction of stable walking for a toy that cannot stand. *Physical Review E*, 64(2):022901, 2001.

[14] M.J. Coleman and A. Ruina. An uncontrolled walking toy that cannot stand still. *Physical Review Letters*, 80(16):3658–3661, 1998.

[15] S. Collins, A. Ruina, R. Tedrake, and M. Wisse. Efficient bipedal robots based on passive-dynamic walkers. *Science*, 307(5712):1082, 2005.

[16] S.H. Collins and A. Ruina. A bipedal walking robot with efficient and human-like gait. In *Proceeding of 2005 International Conference on Robotics and Automation, Barcelona, Spain*, 2005.

[17] S.H. Collins, M. Wisse, and A. Ruina. A three-dimensional passive-dynamic walking robot with two legs and knees. *The International Journal of Robotics Research*, 20(7):607, 2001.

[18] E. Dertien. Dynamic walking with Dribbel. *Robotics & Automation Magazine, IEEE*, 13(3):118–122, 2006.

[19] G.T. Fallis. Walking toy, 1888. U.S. Patent No. 376588.

[20] AM Formalsky. *Impulsive control for anthropomorphic biped*. Springer, 1995.

[21] Robert J Full, Timothy Kubow, John Schmitt, Philip Holmes, and Daniel Koditschek. Quantifying dynamic stability and maneuverability in legged locomotion. *Integrative and comparative biology*, 42(1):149–157, 2002.

[22] Mariano Garcia, Anindya Chatterjee, Andy Ruina, and Michael Coleman. The simplest walking model: stability, complexity, and scaling. *Journal of biomechanical engineering*, 120(2):281–288, 1998.

[23] Mariano Sylvio Garcia. *Stability, scaling, and chaos in passive-dynamic gait models*. PhD thesis, Cornell University, 1999.

[24] Mario Gomes and Andy Ruina. Walking model with no energy cost. *Physical Review E*, 83(3):032901, 2011.

[25] Mario W Gomes and Konrad Ahlin. Quiet (nearly collisionless) robotic walking. In *Robotics and Automation (ICRA), 2015 IEEE International Conference on*, pages 5761–5766. IEEE, 2015.

[26] Ambarish Goswami, Bernard Espiau, and Ahmed Keramane. Limit cycles in a passive compass gait biped and passivity-mimicking control laws. *Autonomous Robots*, 4(3):273–286, 1997.

[27] Ambarish Goswami, Benoit Thuilot, and Bernard Espiau. A study of the passive gait of a compass-like biped robot: symmetry and chaos. *International Journal of Robotics Research*, 17(12):1282–1301, 1998.

[28] Fabian Guenther and Fumiya IIda. Energy efficient monopod running with large payload based on open loop parallel elastic actuation. *Transactions on Robotics*, 2016 (submitted).

[29] Daan GE Hobbelen. *Limit cycle walking*. TU Delft, Delft University of Technology, 2008.

[30] Devin L Jindrich and ROBERT J Full. Many-legged maneuverability: dynamics of turning in hexapods. *The Journal of experimental biology*, 202(12):1603–1623, 1999.

[31] Matthew Kelly and Andy Ruina. Non-linear robust control for inverted-pendulum 2d walking. In *Robotics and Automation (ICRA), 2015 IEEE International Conference on*, pages 4353–4358. IEEE, 2015.

[32] Myunghee Kim and Steven Collins. Once-per-step control of ankle push-off work improves balance in a three-dimensional simulation of bipedal walking. *Robotics, IEEE Transactions on*, 2016 (in press).

[33] Arthur D Kuo. Stabilization of lateral motion in passive dynamic walking. *The International journal of robotics research*, 18(9):917–930, 1999.

[34] Arthur D Kuo. Energetics of actively powered locomotion using the simplest walking model. *Transactions-American Society of Mechanical Engineers Journal of Biomechanical Engineering*, 124(1):113–120, 2002.

[35] Arthur D Kuo. Choosing your steps carefully. *Robotics & Automation Magazine, IEEE*, 14(2):18–29, 2007.

[36] J. J. Mahan and J. F. Moran. Toy, 1909. U.S. Patent No. 1007316.

[37] R. Margaria. Positive and negative work performances and their efficiencies in human locomotion. *European Journal of Applied Physiology and Occupational Physiology*, 25(4):339–351, 1968.

[38] T. McGeer. Passive dynamic walking. *The International Journal of Robotics Research*, 9(2):62, 1990.

[39] Tad McGeer. Passive dynamic biped catalogue, 1991. In *Experimental Robotics II*, pages 463–490. Springer, 1993.

[40] H. Miura and I. Shimoyama. Dynamic walk of a biped. *The International Journal of Robotics Research*, 3(2):60, 1984.

[41] Simon Mochon and Thomas A McMahon. Ballistic walking. *Journal of biomechanics*, 13(1):49–57, 1980.

[42] K.D. Mombaur, H.G. Bock, J.P. Schloder, and R.W. Longman. Human-like actuated walking that is asymptotically stable without feedback. In *International Conference on Robotics and Automation, Seoul, Korea*, pages 4128–4133, 2001.

[43] Katsuhiko Ogata. *Discrete-time control systems*, volume 2. Prentice Hall Englewood Cliffs, NJ, 1995.

[44] Dai Owaki, Masatoshi Koyama, Shinichi Yamaguchi, Shota Kubo, and Akio Ishiguro. A 2-d passive-dynamic-running biped with elastic elements. *Robotics, IEEE Transactions on*, 27(1):156–162, 2011.

[45] A. Ruina. Cornell ranger 2011, 4-legged bipedal robot. `http://ruina.tam.cornell.edu/research/topics/locomotion_and_robotics/ranger/Ranger2011/` or google search for cornell ranger, April 2012 2012.

[46] A. Ruina, J.E.A. Bertram, and M. Srinivasan. A collisional model of the energetic cost of support work qualitatively explains leg sequencing in walking and galloping, pseudo-elastic leg behavior in running and the walk-to-run transition. *Journal of theoretical biology*, 237(2):170–192, 2005.

[47] Steven H Strogatz. *Nonlinear dynamics and chaos: with applications to physics, biology, chemistry, and engineering*. Westview press, 2014.

[48] Vance A Tucker. Energetic cost of locomotion in animals. *Comparative Biochemistry and Physiology*, 34(4):841–846, 1970.

[49] J. E. Wilson. Walking toy, 1938. US Patent 2140275.

[50] Martijn Wisse, Daan GE Hobbelen, and Arend L Schwab. Adding an upper body to passive dynamic walking robots by means of a bisecting hip mechanism. *Robotics, IEEE Transactions on*, 23(1):112–123, 2007.

[51] Martijn Wisse and Arend L Schwab. First steps in passive dynamic walking. In *Climbing and Walking Robots*, pages 745–756. Springer, 2005.

[52] Martijn Wisse, Arend L Schwab, Richard Quint van der Linde, and Frans CT van der Helm. How to keep from falling forward: elementary swing leg action for passive dynamic walkers. *Robotics, IEEE Transactions on*, 21(3):393–401, 2005.